Driven-Base Tests for Modal Parameter Estimation

F. R. Vigneron* and Y. Soucy†
Communications Research Center, Ottawa, Canada

The theory for parameter estimation from driven-base tests is outlined. The parameters that can be estimated from accelerometer data of the driven base and of points on the structure under test are found to be, for each mode, the modal frequency, the modal damping factor, the mode shape, and the products (modal momentum coefficient × modal scale factor). If, in addition, the modal scale factors are obtained from an independent partial modal survey test or from an analytical model, then estimates of the modal momentum coefficients can be constructed. The modal momentum coefficients can then be used, in conjunction with modal identities, to assess the relative significance and overall completeness of the experimentally-determined modes. The parameter estimation and use of modal identities are illustrated with data from a simulated structure.

I. Introduction

IN the space vehicle industry, structural qualification is often determined with a dynamic test in which the structure is attached to a rigid platform (base) that is driven in a single translational direction by a powerful electrodynamic or hydraulic exciter system. The input measurement is made with an accelerometer mounted to the base, and the measured outputs are defined as accelerations at several points on the structure. The main purpose of this "driven-base test" is to subject the structure to vibration environments that are similar to those to be experienced during launch. Similar dynamic tests are employed for qualifying equipment in the nuclear industry, using a platform that is simultaneously driven in three translational and three rotational directions. Six-degree-of-freedom test facilities are also under development for space.[1]

Until recently, the extraction of modal parameters from data of driven-base tests had not been done rigorously and accurately. However, the possibility of doing so is attractive to agencies who presently use driven-base qualification testing because the parameter extraction process could be added to the conventional environmental test sequences at little cost. Also, in driven-base modal tests, stinger rods, load cells, and any associated special holes in the structure would not be required—an important factor in testing complex compact structures. Motivated by these considerations, procedures to determine modal frequencies, modal damping factors, and mode shapes have been established from driven-base tests.[2,3] The work addresses the case where the excitation in a specific test is in a single translational direction.

The dynamic and measurement configuration of the previously discussed driven-base test is different than that of the "modal test" (also referred to as the "modal survey test"). The latter involves supporting the structure with respect to a nonmovable reference, and exciting it with exciters (small portable electrodynamic or hydraulic vibrators, or an impluse hammer) at one or more points on the structure. Measured inputs are the exciter forces, and the measured outputs are accelerations at several points on the structure. The modal survey test has the identification of structural parameters as its main objective. The identifiable parameters are the modal frequencies, modal damping factors, mode shapes, and modal normalization constants (or equivalently, the modal masses).[4,5]

The work reported in this paper was originally motivated by a desire to clarify the role of the driven-base test in estimating modal mass. However, the results have led to the realization that the potential of the driven-base test is considerably greater than that of an alternate to the modal survey tests, as was envisaged originally. It turns out that the driven-base test yields estimates of the product (modal linear momentum coefficient × modal normalization constant) for each mode. If the normalization constants are obtained separately, either by a partial modal survey test or from an analytical model, it becomes possible to calculate experimental estimates of the modal linear momentum coefficients. The experimentally derived modal momentum coefficients can be used in conjunction with modal identities for damped natural modes[6,7] to assess the relative significance of individual modes and the overall completeness of the experimental modal determination.

In this paper, the basic modal models are given in a form that makes clear the role of the modal momentum coefficients and normalization constants in parameter estimation using driven-base data. The parameter estimation procedures and the results described in the preceding paragraph are illustrated using data generated with a computer simulation of a structure.

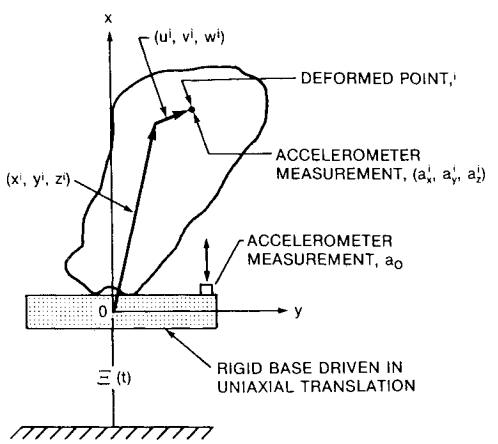

Fig. 1 Schematic of driven base and attached structure.

Received Oct. 28, 1985; presented as Paper 86-0870 at the AIAA/ASME/ASCE/AHS 27th Structures, Structural Dynamics and Materials Conference, San Antonio, TX, May 19-21, 1986; revision received April 20, 1986.

*Research Scientist. Member AIAA.
†Research Engineer. Member AIAA.

II. Parameter Estimation—Driven-Base Excitation in Single-Degree-of-Freedom Translation

Model in Terms of Physical Variables

The driven-base and attached structure are shown schematically in Fig. 1. The base is assumed to be rigid and driven in a single direction, Ox, with no rotation. The attached structure is modeled by N mass points, each with mass m^i and location x^i, y^i, z^i, in the undeformed state. The reference axes Ox, Oy, Oz, are arbitrarily fixed to a convenient location on the driven-base. The deformation of each mass point is defined relative to the driven-base by components (u^i, v^i, w^i) in the (Ox, Oy, Oz) reference frame.

The measureable quantities upon which parameter estimation is based are: 1) the input acceleration, $a_0(t)$, equal to $\ddot{\Xi}(t)$; and 2) the inertial accelerations at each mass point denoted by $\{a_x^i(t), a_y^i(t), a_z^i(t)\}$. The symbol t denotes time.

The following column matrices are defined

$$U = \begin{bmatrix} u^1 \\ u^2 \\ u^3 \\ \vdots \\ u^N \end{bmatrix} \quad A_x = \begin{bmatrix} a_x^1 \\ a_x^2 \\ a_x^3 \\ \vdots \\ a_x^N \end{bmatrix} \quad \Sigma = \begin{bmatrix} 1 \\ 1 \\ 1 \\ \vdots \\ 1 \end{bmatrix} \tag{1}$$

and similarly for V, W, A_y, and A_z. Then, the relationship between the measureable quantities (accelerations) and the deformation variables may be written as

$$\begin{bmatrix} A_x(t) \\ A_y(t) \\ A_z(t) \end{bmatrix} = \begin{bmatrix} \ddot{U}(t) \\ \ddot{V}(t) \\ \ddot{W}(t) \end{bmatrix} + \begin{bmatrix} \Sigma \\ 0 \\ 0 \end{bmatrix} a_0(t) \tag{2}$$

The matrices U, A_x, Σ, 0, etc. are all of order $N \times 1$.

The motion equations for the structure can be readily deduced from the first principles as

$$M \begin{bmatrix} \ddot{U} \\ \ddot{V} \\ \ddot{W} \end{bmatrix} + C \begin{bmatrix} \dot{U} \\ \dot{V} \\ \dot{W} \end{bmatrix} + K \begin{bmatrix} U \\ V \\ W \end{bmatrix} = - \begin{bmatrix} M^N \Sigma \\ 0 \\ 0 \end{bmatrix} a_0(t) \tag{3}$$

In the above, C and K are damping and stiffness matrices, respectively, and are of order $3N \times 3N$. M^N is of order $N \times N$, and is diagonal with elements $m^1, m^2, m^3, \ldots m^N$. M is the mass matrix, and is diagonal and of order $3N \times 3N$;

$$M = \begin{bmatrix} M^N & 0 & 0 \\ 0 & M^N & 0 \\ 0 & 0 & M^N \end{bmatrix} \tag{4}$$

The relative accelerations of Eqs. (3), $\ddot{U}$, $\ddot{V}$, and $\ddot{W}$, are not directly measurable. Equation (2) provides the transformation from the measurable absolute accelerations to the relative ones. Fourier transformation of Eqs. (2) and (3) (with zero initial conditions) leads to

$$\begin{bmatrix} \bar{A}_x(\omega) - \Sigma \bar{a}_0(\omega) \\ \bar{A}_y(\omega) \\ \bar{A}_z(\omega) \end{bmatrix} = \omega^2 \bar{H}(\omega) \begin{bmatrix} M^N \Sigma \\ 0 \\ 0 \end{bmatrix} \bar{a}_0(\omega) \tag{5}$$

where ω is the frequency variable and $\bar{H}(\omega)$ is the frequency response function

$$\bar{H}(\omega) = [-\omega^2 M + i\omega C + K]^{-1} \tag{6}$$

Model in Terms of Damped Modal Variables

The frequency response function, which is expressed in terms of physical parameters in Eq. (6), may be expressed in terms of modal parameters λ_k, Φ_k, Q_k, and $k = 1$ to n as[6,7]

$$\bar{H}(\omega) = \sum_{k=1}^{n} \left\{ \frac{Q_k \Phi_k \Phi_k^T}{(i\omega - \lambda_k)} + \frac{Q_k^* \Phi_k^* \Phi_k^{*T}}{(i\omega - \lambda_k^*)} \right\} \tag{7}$$

where n is the number of modes of the system and is equal to $3N$. λ_k and Φ_k are the complex eigenvalue and mode shape, respectively, of the kth mode, and are obtained from solution of the eigenvalue problem

$$[M\lambda_k^2 + C\lambda_k + K]\Phi_k = 0 \tag{8}$$

Q_k is the modal normalization constant of the kth mode

$$Q_k = \{\Phi_k^T (2\lambda_k M + C)\Phi_k\}^{-1} \tag{9}$$

The symbol $(*)$ denotes complex conjugate. The Φ_k are complex-valued column matrices of order $n \times 1$. The Q_k are complex-valued scalars.

An eigenvalue is related to its modal frequency ω_k, and modal damping factor ζ_k, by $\lambda_k = -\zeta_k \omega_k + i\omega_k (1 - \zeta_k^2)^{1/2}$. A mode shape, Φ_k, further has a structure

$$\Phi_k = \begin{bmatrix} \theta_k \\ \phi_k \\ \psi_k \end{bmatrix} \tag{10}$$

where θ_k, ϕ_k, and ψ_k are the components ($N \times 1$ matrices) in the Ox, Oy, and Oz directions, respectively.

Substitution of Eq. (7) into Eq. (5), with some rearrangement, yields

$$\frac{1}{\omega^2} \begin{bmatrix} \bar{A}_x(\omega)/\bar{a}_0(\omega) - \Sigma \\ \bar{A}_y(\omega)/\bar{a}_0(\omega) \\ \bar{A}_z(\omega)/\bar{a}_0(\omega) \end{bmatrix} = \sum_{k=1}^{n} \left\{ \frac{Q_k \mathcal{P}_{xk} \Phi_k}{i\omega - \lambda_k} + \frac{Q_k^* \mathcal{P}_{xk}^* \Phi_k^*}{i\omega - \lambda_k^*} \right\} \tag{11}$$

where

$$\mathcal{P}_{xk} = \Sigma^T M^N \theta_k = \sum_{i=1}^{N} m^i \theta_k^i \tag{12}$$

$\mathcal{P}_{xk}$ is a modal parameter, namely, the linear modal momentum coefficient of the kth mode. Eq. (11) relates the modal parameters (right-hand side, λ_k, Φ_k, Q_k, and $\mathcal{P}_{xk}$, $k = 1$ to n) to the quantities that are directly measureable (left-hand side, A and a_0). It is the basic model needed for parameter estimation by curve-fitting methods for driven-base tests with single-degree-of-freedom excitation in the Ox direction.

For proportional damping, the Φ_k turns out to be real-valued. If damping is also light, then $\lambda_k \simeq i\omega_k$ and Eq. (9) approximates to $Q_k \simeq (2i\omega_k m_k)^{-1}$, where m_k is the modal mass of the kth mode and equals the real-valued quantity $\Phi_k^T M \Phi_k$. The $\mathcal{P}_{xk}$ are also real-valued. Equation (11) then reduces to

$$\frac{1}{\omega^2} \begin{bmatrix} \bar{A}_x(\omega)/\bar{a}_0(\omega) - \Sigma \\ \bar{A}_y(\omega)/\bar{a}_0(\omega) \\ \bar{A}_z(\omega)/\bar{a}_0(\omega) \end{bmatrix}$$

$$= \sum_{k=1}^{n} \frac{\mathcal{P}_{xk} \Phi_k}{2im_k \omega_k} \left\{ \frac{1}{(i\omega - \lambda_k)} - \frac{1}{(i\omega - \lambda_k^*)} \right\} \tag{13}$$

Table 1 Comparison of estimated undamped frequencies and damping ratios—driven-base test in *Ox* direction

Mode	Driving point	Frequency, Hz		Damping ratio	
		Theoretical	Estimated	Theoretical	Estimated
1	4*x*	3.781	3.781	0.04279	0.04279
2	4*x*	5.918	5.918	0.05196	0.05196
3	4*x*	10.25	10.25	0.09524	0.09525
4	6*z*	33.90	33.90	0.01183	0.01183
5	4*x*	45.84	45.84	0.03015	0.03016
6	4*x*	51.21	51.21	0.05417	0.05418
7	5*z*	59.53	59.53	0.04306	0.04306
8	4*z*	81.42	81.42	0.08462	0.08465
9	4*x*	218.9	218.9	0.00943	0.00943

If the excitation is applied in the *Oy* direction, then the counterpart of Eq. (11) turns out to be

$$\frac{1}{\omega^2}\begin{bmatrix} \bar{A}_x(\omega)/\bar{a}_0(\omega) \\ \bar{A}_y(\omega)/\bar{a}_0(\omega)-\Sigma \\ \bar{A}_z(\omega)/\bar{a}_0(\omega) \end{bmatrix} = \sum_{k=1}^{n}\left\{\frac{Q_k\mathcal{P}_{yk}\Phi_k}{(i\omega-\lambda_k)}+\frac{Q_k^*\mathcal{P}_{yk}^*\Phi_k^*}{(i\omega-\lambda_k^*)}\right\} \tag{14}$$

where

$$\mathcal{P}_{yk}=\Sigma^T M^N\phi_k=\sum_{i=1}^{N} m^i\phi_k^i \tag{15}$$

A parallel equation involving $\mathcal{P}_{zk}$ follows if the excitation is applied in the *Oz* direction.

Modal Parameter Estimation—Driven-Base Test

For a driven-base test with input in the *Ox* direction, estimates of the functions $\bar{A}_x(\omega)/\bar{a}_0(\omega)$, $\bar{A}_y(\omega)/\bar{a}_0(\omega)$, and $\bar{A}_z(\omega)/\bar{a}_0(\omega)$ may be obtained from the accelerometer data using standard data acquisition and spectral analysis equipment. From these functions, a measurement-based estimate of the column matrix function appearing on the left-hand side of Eq. (11) or (13) may be constructed. The "identified" modal parameters are the parameters that result in an acceptable curve fit of Eq. (11) or (13) to the measurement-based estimate of the column matrix function.

For well separated modes, the modal eigenvalues may be obtained from the measurement-based functions by standard single-degree-of-freedom (SDOF) techniques. Equation (13) shows that the mode shape of a *k*th mode is proportional to the measurement-based column. After a choice of the arbitrary scale of Φ_k is made, the constant $\mathcal{P}_{xk}/m_k$ can be determined by calculating it from Eq. (13) at the ω equal to the SDOF-derived ω_k. Unfortunately, there is not enough information to separate $\mathcal{P}_{xk}$ and m_k.

The complex exponentials method offers an alternate parameter estimation method (multi-degree-of-freedom), in conjunction with the modal model in the form given in Eq. (11). In the example in Sec. III, the complex exponentials algorithm (implemented in commercially available software) was employed.[8,9] With the algorithm and software, estimates of the λ_k and B_k are derived, which result in a curve fit of an equation of the form

$$Y(\omega)=\sum_{k=1}^{2n}\frac{B_k}{i\omega-\lambda_k} \tag{16}$$

to the measurement-based column matrix $Y(\omega)$ that corresponds to the left-hand side of Eq. (11). (The superscript $\hat{}$ denotes a numerical estimate, i.e., a number.) By comparing Eq. (11) and Eq. (16), a mode shape, Φ_k, is seen to be proportional to an estimate $\hat{B}_k$, i.e.,

$$Q_k\mathcal{P}_{xk}\Phi_k=\hat{B}_{xk} \tag{17}$$

If the *d*th element of $\Phi_k(\Phi_k^d)$ is specified to have the value $1+i0$, then an estimate for $Q_k\mathcal{P}_{xk}$ is given by

$$\widehat{(Q_k\mathcal{P}_{xk})}=\hat{B}_{xk}^d \tag{18}$$

and for Φ_k, by

$$\hat{\Phi}_k=\frac{1}{\hat{B}_{xk}^d}\hat{B}_{xk} \tag{19}$$

Thus, as in the preceding subsection with the proportionally-damped model and an SDOF technique, there is not enough information to make separate estimates of Q_k and $\mathcal{P}_{xk}$ for a particular mode solely from the data of the driven-base test as defined herein.

In a similar manner, estimates of $\widehat{(Q_k\mathcal{P}_{yk})}$ and $\widehat{(Q_k\mathcal{P}_{zk})}$ can be made from data of driven-base tests with excitation in the *Oy* and *Oz* directions, respectively.

Equations (11) and (14) can be combined into a single matrix equation. Then a matrix form of the complex exponentials method may be used to simultaneously process test results from two single axes tests with excitation in the *Ox* and *Oy* directions, respectively. As before, λ_k, Φ_k, and products $Q_k\mathcal{P}_{xk}$ and $Q_k\mathcal{P}_{yk}$ can be estimated. Likewise, the results of three single axis tests could also be simultaneously processed if desired.

The modal parameters estimated in the driven-base tests, namely λ_k, Φ_k, $(Q_k\mathcal{P}_{xk})$, $(Q_k\mathcal{P}_{yk})$, and $(Q_k\mathcal{P}_{zk})$, correspond to the eigenvalue problem of Eq. (8), and are the fixed-base damped natural modes of the structure. As will be seen in the next section, the modal parameters extracted from a modal survey test correspond to the same eigenvalue problem and fixed-base damped natural modes.

Estimation of the Q_k from Modal Survey Test

In a modal survey test, a single force exciter inputs a force, $f_0(t)$, at a driving location corresponding to the *d*th element of the matrix $q=[U^T,V^T,W^T]^T$. The force may be represented as $f(t)=E_f f_0(t)$, where E_f is an $n\times 1$ column matrix with zeros at every element except the location corresponding to the driving point, at which the element is unity. In the test, the acceleration $a(t)=[A_x^T(t),A_y^T(t),A_z^T(t)]^T$, equal to $\ddot{q}(t)$, is the output measurement. The transfer function, Eq. (7), is defined such that $\bar{q}(\omega)=\bar{H}(\omega)\bar{f}(\omega)$, and $\bar{a}(\omega)=-\omega^2\bar{q}(\omega)$. Combining these relationships and Eq. (7)

leads to

$$\begin{bmatrix} \bar{A}_x(\omega) \\ \bar{A}_y(\omega) \\ \bar{A}_z(\omega) \end{bmatrix} = -\omega^2 \sum_{k=1}^{n} \left\{ \frac{Q_k \Phi_k \Phi_k^T}{(i\omega - \lambda_k)} + \frac{Q_k \Phi_k^* \Phi_k^{*T}}{(i\omega - \lambda_k^*)} \right\} E_f \bar{f}_0(\omega) \tag{20}$$

Since $\Phi_k^T E_f$ equals Φ_k^d, namely the element of the mode shape of the driving point coordinate, the above equation takes the form

$$-\frac{1}{\omega^2} \begin{bmatrix} \bar{A}_x(\omega)/\bar{f}_0(\omega) \\ \bar{A}_y(\omega)/\bar{f}_0(\omega) \\ \bar{A}_z(\omega)/\bar{f}_0(\omega) \end{bmatrix} = \sum_{k=1}^{n} \left\{ \frac{Q_k \Phi_k^d \Phi_k}{(i\omega - \lambda_k)} + \frac{Q_k^* \Phi_k^{d*} \Phi_k^*}{(i\omega - \lambda_k^*)} \right\} \tag{21}$$

Equation (21) is the counterpart of Eq. (11). The two equations have the same form in the right-hand side, with $\mathcal{P}_{xk}$ appearing in Eq. (11) where $\Phi_k{}^d$ appears in Eq. (21).

For proportional damping, Eq. (21) further reduces to

$$-\frac{1}{\omega^2} \begin{bmatrix} \bar{A}_x(\omega)/\bar{f}_0(\omega) \\ \bar{A}_y(\omega)/\bar{f}_0(\omega) \\ \bar{A}_z(\omega)/\bar{f}_0(\omega) \end{bmatrix} = \sum_{k=1}^{n} \frac{\Phi_k^d \Phi_k}{2im_k\omega_k} \left\{ \frac{1}{(i\omega - \lambda_k)} - \frac{1}{(i\omega - \lambda_k^*)} \right\} \tag{22}$$

Equation (22) is consistent with Refs. 4 and 5 regarding definition of modal mass and other parameters, and is based on a proportionally-damped linear viscous model. Estimation with this model leads to estimates of the m_k, λ_k, and Φ_k.

The application of the curve fitting procedure described in Eqs. (16-19) to the general model Eq. (21), results in estimates of the general parameter Q_k (instead of the m_k),

Table 2 Comparison of estimate of $(Q_k\mathcal{P}_{xk})\hat{}$ and $Q_k\mathcal{P}_{xk}$—driven-base test in *Ox* direction

	Amplitude			Phase, deg		
Mode	$\lvert Q_k\mathcal{P}_{xk}\rvert$	$\lvert(Q_k\mathcal{P}_{xk})\hat{}\rvert$	Error, %	$\angle Q_k\mathcal{P}_{xk}$	$\angle(Q_k\mathcal{P}_{xk})\hat{}$	Diff.
1	0.3651 *E*-2	0.3651 *E*-2	0.0	88.45	88.46	0.01
2	0.6960 *E*-2	0.6960 *E*-2	0.0	−94.78	−94.77	0.01
3	0.4791 *E*-2	0.4791 *E*-2	0.0	−85.81	−85.83	−0.02
4	0.1363 *E*-3	0.1363 *E*-3	0.0	91.17	91.16	−0.01
5	0.7107 *E*-4	0.7110 *E*-4	0.0	−14.60	−14.61	−0.01
6	0.8819 *E*-4	0.8830 *E*-4	0.1	−44.62	−44.58	0.04
7	0.1596 *E*-3	0.1596 *E*-3	0.0	−89.96	−89.95	0.01
8	0.7627 *E*-5	0.7640 *E*-5	0.2	10.42	10.49	0.07
9	0.9973 *E*-6	0.9987 *E*-6	0.1	7.49	7.45	−0.04

Table 3 Difference between MAC $(\Phi_i, \hat{\Phi}_k)$ and MAC $(\Phi_i\Phi_k)$—excitation in the *Ox* direction[a]

	Mode								
	$\hat{1}$	$\hat{2}$	$\hat{3}$	$\hat{4}$	$\hat{5}$	$\hat{6}$	$\hat{7}$	$\hat{8}$	$\hat{9}$
1	0.00000	0.00001	0.00004	0.00000	0.00003	0.00111	0.00003	0.00011	0.00002
2	0.00000	0.00000	0.00006	0.00000	0.00007	0.00182	0.00003	0.00038	0.00005
3	0.00001	0.00001	0.00000	0.00001	0.00008	0.00036	0.00003	0.00469	0.00031
4	0.00000	0.00000	0.00000	0.00000	0.00002	0.00011	0.00000	0.00005	0.00000
5	0.00001	0.00005	0.00021	0.00001	0.00000	0.00051	0.00004	0.00280	0.00019
6	0.00002	0.00001	0.00000	0.00000	0.00002	0.00116	0.00013	0.00670	0.00009
7	0.00000	0.00000	0.00000	0.00000	0.00001	0.00149	0.00000	0.00075	0.00001
8	0.00000	0.00000	0.00001	0.00000	0.00002	0.00006	0.00002	0.00449	0.00000
9	0.00001	0.00000	0.00006	0.00000	0.00007	0.00006	0.00005	0.00219	0.00000

[a]The value of MAC is 1 for two dependent mode shapes.

Table 4 Comparison of estimates of $(Q_k\mathcal{P}_{yk})\hat{}$ and $Q_k\mathcal{P}_{yk}$—driven-base test in *Oy* direction

	Amplitude			Phase, deg		
Mode	$\lvert Q_k\mathcal{P}_{yk}\rvert$	$\lvert(Q_k\mathcal{P}_{yk})\hat{}\rvert$	Error, %	$\angle Q_k\mathcal{P}_{yk}$	$\angle(Q_k\mathcal{P}_{yk})\hat{}$	Diff.
1	0.6043 *E*-2	0.6043 *E*-2	0.0	89.70	89.73	0.03
2	0.4527 *E*-2	0.4526 *E*-2	0.0	84.40	84.40	0.00
3	0.5043 *E*-2	0.5041 *E*-2	0.0	−94.70	−94.65	0.05
4	0.7694 *E*-4	0.7694 *E*-4	0.0	−90.74	−90.76	−0.02
5	0.1027 *E*-4	0.1025 *E*-4	−0.2	70.12	70.07	−0.05
6	0.7651 *E*-4	0.7653 *E*-4	0.0	−164.83	−164.84	−0.01
7	0.8610 *E*-4	0.8612 *E*-4	0.0	−86.22	−86.29	−0.07
8	0.2212 *E*-3	0.2209 *E*-3	−0.1	82.62	82.68	0.06
9	0.2545 *E*-5	0.2546 *E*-5	0.0	−26.39	−26.36	−0.3

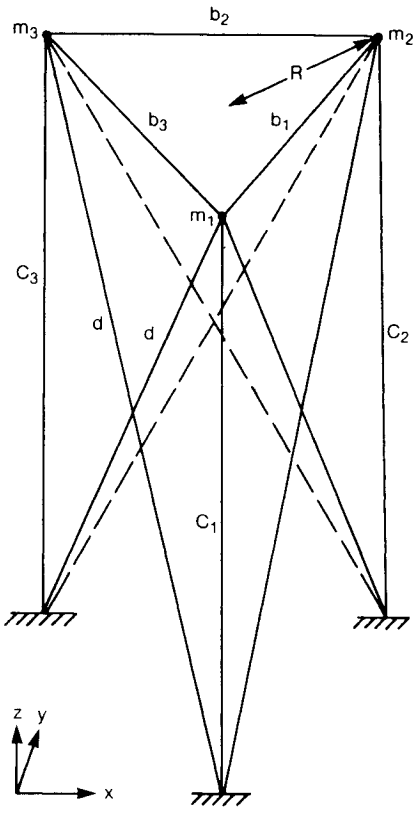

R = 5 in
HEIGHT = 20 in
MASS OF m_1 = 0.1 lb-sec^2/in
MASS OF m_2 = 0.3 lb-sec^2/in
MASS OF m_3 = 2.0 lb-sec^2/in
EA OF d = 0.2 × 10^6 lb
EA OF b_1 = 1.2 × 10^6 lb
EA OF b_2 = 0.2 × 10^6 lb
EA OF b_3 = 0.1 × 10^6 lb
EA OF c_1 = 0.2 × 10^6 lb
EA OF c_2 = 0.5 × 10^6 lb
EA OF c_3 = 1.5 × 10^6 lb

$$\text{DAMPING MATRIX} = \begin{bmatrix} .04 & & & & & & \\ & .05 & & & & & \\ & & .03 & & & & \\ & & & .03 & & & \\ & & & & .008 & & \\ & & & & & .02 & \\ & & & & & & .09 \\ & & & & & & & .1 \\ & & & & & & & & .1 \end{bmatrix}$$

Fig. 2 Simulated structure.

and the λ_k and Φ_k. More specifically, we denote the estimates of eigenvalue and amplitude that result in a curve fit of Eq. (16) to the data $A_x(\omega)/[\omega^2 f_0(\omega)]$, etc. as $\hat{\lambda}_k$ and $\hat{R}_k$. Then from Eq. (21)

$$Q_k \Phi_k^d \Phi_k = \hat{R}_k \tag{23}$$

If Φ_k^d is assigned a value $1 + i0$, then an estimate of Q_k is given by

$$\hat{Q}_k = \hat{R}_k^d \tag{24}$$

and for Φ_k by

$$\hat{\Phi}_k = \frac{1}{\hat{R}_k^d} \hat{R}_k \tag{25}$$

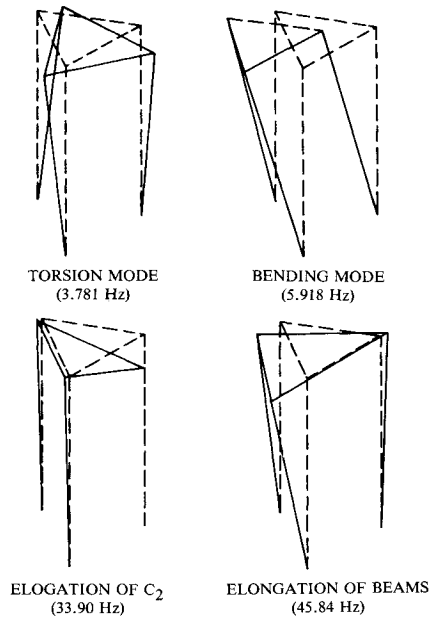

Fig. 3 Sample of mode shapes.

In principle, the $\hat{Q}_k$ can be obtained from a single instrumented point on the structure. A scale factor Q_k is dependent on the choice of the driving point. To estimate Φ_k, output measurements are needed at multiple points.

Estimates for the $\mathcal{P}_{xk}$

A driven-base test with excitation in the Ox direction leads to an estimate of products, $\widehat{(Q_k \mathcal{P}_{xk})}$ [Eq. (18)]. If a modal survey test is also done, estimates for the Q_k can be obtained via Eq. (24). Combining these yields estimates for $\mathcal{P}_{xk}$

$$\hat{\mathcal{P}}_{xk} = \frac{\widehat{(Q_k \mathcal{P}_{xk})}}{\hat{Q}_k} \tag{26}$$

Likewise, estimates $\hat{\mathcal{P}}_{yk}$ and $\hat{\mathcal{P}}_{zk}$ can be obtained from driven-base tests with excitation in the Oy and Oz directions. As an alternate to a modal survey test, estimates for the Q_k could also be derived from an analytical model using Eq. (9).

The following points are important to note. In principle, the $\hat{Q}_k$ can be obtained in a modal survey test from a single output accelerometer located at a point that is not a node of one of the vibrational modes (as can estimates, $\hat{\lambda}_k$, as is well known). Likewise, estimates of $\widehat{(Q_k \mathcal{P}_{xk})}$ can be obtained in a driven-base test from the same single test point. (In a practical test, to avoid low signals at locations near nodes and for verification purposes, more than a single point might be required, but not as many as for measurement of mode shapes.) It thus follows that the accuracy of the estimates, $\hat{\mathcal{P}}_{xk}$, does not depend on the order or manner of the discretization of the earlier-defined physical model.

Modal Identities

The modal identities of Refs. 6 and 7 may be written in the form

$$\sum_{k=1}^{n} \mathfrak{M}_{xx}^k \le m \qquad \sum_{k=1}^{n} \mathfrak{M}_{xy}^k \le 0 \qquad \sum_{k=1}^{n} \mathfrak{M}_{xz}^k \le 0$$

$$\sum_{k=1}^{n} \mathfrak{M}_{yy}^k \le m \qquad \sum_{k=1}^{n} \mathfrak{M}_{yz}^k \le 0$$

$$\sum_{k=1}^{n} \mathfrak{M}_{zz}^k \le m \tag{27}$$

where

$$\mathfrak{M}^k_{xx} = \lambda_k Q_k \mathcal{P}^2_{xk} + \lambda^*_k Q^*_k \mathcal{P}^{*2}_{xk} \tag{28a}$$

$$\mathfrak{M}^k_{xy} = \lambda_k Q_k \mathcal{P}_{xk} \mathcal{P}_{yk} + \lambda^*_k Q^*_k \mathcal{P}^*_{xk} \mathcal{P}^*_{yk} \tag{28b}$$

and so forth for $\mathfrak{M}^k_{xz}$, $\mathfrak{M}^k_{yy}$, $\mathfrak{M}^k_{yz}$, and $\mathfrak{M}^k_{zz}$. The values $\mathfrak{M}^k_{xx}$, $\mathfrak{M}^k_{xy}$, etc., may be shown to be invariant to the choice of scale factor $\Phi_{\ell k}$ (i.e., the driving point).

Estimates $\hat{\lambda}_k$, $\hat{Q}_k$, $\hat{\mathcal{P}}_{xk}$, etc. can be derived from the previously outlined tests, and hence experimentally based estimates for $\hat{\mathfrak{M}}^k_{xx}$, $\hat{\mathfrak{M}}^k_{xy}$, etc. can be calculated using Eq. (28). The mass m of the structure can be estimated by weighing it or by calculation.

Comparison of the individual $\hat{\mathfrak{M}}^k_{xx}$, $k = 1,2$, etc. gives an indication of the relative linear momenta in the x direction associated with each mode (similarly for $\hat{\mathfrak{M}}^k_{yy}$ and $\hat{\mathfrak{M}}^k_{zz}$, and the y and z directions, respectively). Comparison of the sums of the estimates indicated in Eq. (27), relative to m and zero, gives an indication of the completeness and accuracy of the experimental modal determination process. These principles are illustrated in the example to follow.

III. Example with Simulated Data

Simulated Structure

A finite-element model of the structure depicted in Fig. 2 was prepared to generate simulated data for estimation and to present theoretical results for comparison to estimated ones. The structure consists of three masses, interconnected and connected to ground with axial elements. Each element includes nonproportional damping. The analytical model produces nine damped natural modes, of which four are represented in Fig. 3. The parameters λ_k, Φ_k, B_{xk}, Q_k, $\mathcal{P}_{xk}$, $\mathcal{P}_{yk}$, R^k, etc. were calculated for subsequent comparison with the estimates for the same parameters.

Estimation from Driven-Base Tests

Simulated response function data corresponding to driven-base tests with input in the *Ox, Oy,* and *Oz* directions were prepared, using Eqs. (5) and (6). In each case, the output acceleration responses were assumed to be measured at each mass point in the *Ox, Oy,* and *Oz* directions. The frequency range containing the nine modal frequencies was divided into six subranges, in which response functions with 512 lines were calculated to accommodate zoomed parameter estimation.

The complex exponentials algorithm of the software described in Ref. 8 was used to estimate the parameters from the simulated data. First, estimates of the λ_k were obtained on the basis of a single response function at locations corresponding to the driving point of the modal survey to be described later on. Then, estimates of the elements of the column matrices, $\hat{B}^i_k$, were obtained sequentially from all the response functions.

The results pertaining to driving in the *Ox* direction are given in Tables 1-3. In Table 1, the estimated modal frequencies and damping ratios are seen to agree with the theoretical results almost perfectly. The estimates of B^d_{xk} which are, in turn, the estimates of $(Q_k \mathcal{P}_{xk})\hat{}$ [Eq. (17)] compare very well with the corresponding theoretical ones, as is demonstrated in Table 2. The estimated mode shapes are compared with the theoretical ones using the modal assurance criterion (MAC)[10] in Table 3. The difference between MAC $(\Phi_i, \hat{\Phi}_k)$ and MAC (Φ_i, Φ_k) is very small, which indicates very good agreement.

Similar results were obtained for the simulated tests with base excitation in the *Oy* and *Oz* directions. Comparison of $Q_k \mathcal{P}_k$ for these cases is given in Tables 4 and 5. The agreement between estimated and theoretical quantities is very good.

Estimation of the Q_k

To obtain estimates of the Q_k, a modal survey test was simulated. Simulated response functions were prepared with the same frequency sub-bands as for the driven-base test. Driving points were selected based on the quality of the peaks of the response functions, and the desire to minimize

Table 5 Comparison of estimates of $(Q_k \mathcal{P}_{zk})\hat{}$ and $Q_k \mathcal{P}_{zk}$—driven-base test in *Oz* direction

	Amplitude			Phase, deg		
Mode	$\lvert Q_k \mathcal{P}_{zk} \rvert$	$\lvert (Q_k \mathcal{P}_{zk})\hat{} \rvert$	Error, %	$\angle Q_k \mathcal{P}_{zk}$	$\angle (Q_k \mathcal{P}_{zk})\hat{}$	Diff.
1	0.3379 *E*-4	0.3379 *E*-4	0.0	−85.81	−85.83	−0.02
2	0.3541 *E*-3	0.3541 *E*-3	0.0	−94.66	−94.65	−0.01
3	0.4038 *E*-4	0.4029 *E*-4	−0.2	33.77	33.86	0.09
4	0.2344 *E*-2	0.2344 *E*-2	0.0	−90.01	−90.01	0.00
5	0.1556 *E*-3	0.1557 *E*-3	0.1	85.46	85.43	−0.03
6	0.1652 *E*-3	0.1644 *E*-3	−0.5	−93.66	−94.25	−0.59
7	0.1260 *E*-2	0.1258 *E*-2	−0.2	−89.58	−89.55	0.03
8	0.9025 *E*-3	0.9025 *E*-3	0.0	−88.02	−88.01	0.01
9	0.5269 *E*-5	0.5269 *E*-5	0.0	92.99	92.99	0.00

Table 6 Comparison of Q_k and $\hat{Q}_k$—modal survey test

	Amplitude			Phase, deg		
Mode	$\lvert Q_k \rvert$	$\lvert \hat{Q}_k \rvert$	Error, %	$\angle Q_k$	$\angle \hat{Q}_k$	Diff.
1	0.1169 *E*-2	0.1169 *E*-2	0.0	−91.44	−91.44	0.00
2	0.2153 *E*-2	0.2153 *E*-2	0.0	−99.87	−99.87	0.00
3	0.1615 *E*-1	0.1614 *E*-1	0.0	−90.24	−90.18	0.06
4	0.1169 *E*-2	0.1169 *E*-2	0.0	−89.99	−90.01	−0.02
5	0.1835 *E*-2	0.1833 *E*-2	−0.1	−97.95	−97.98	−0.03
6	0.7508 *E*-2	0.7520 *E*-2	0.1	−84.30	−84.34	−0.04
7	0.4030 *E*-2	0.4031 *E*-2	0.0	−89.02	−88.92	0.10
8	0.9305 *E*-2	0.9295 *E*-2	−0.1	−88.80	−88.69	0.11
9	0.6110 *E*-3	0.6111 *E*-3	0.0	−88.83	−88.81	0.02

the number of driving points, as would be done in an actual test.

The λ_k were estimated with virtually no error. The comparison between $\hat{Q}_k$, as estimated by Eq. (24) and the theoretical Q_k, is excellent (see Table 6).

From the previously mentioned estimates of $(Q_k \mathcal{P}_{xk})\hat{}$, and $\hat{Q}_k$, one can obtain estimates for $\hat{\mathcal{P}}_{xk}$ [Eq. (26)]. The comparison with theoretical quantities in Table 7 shows that the correspondance is excellent both in amplitude and in phase. Estimates for $\mathcal{P}_{yk}$ made from data of the Oy driven-base tests are of similar quality. Estimates for $\mathcal{P}_{zk}$ are of excellent quality in amplitude and are very good in phase with a maximum error of. 1.4 deg. Table 8 summarizes $\hat{\mathcal{P}}_{xk}$, $\hat{\mathcal{P}}_{yk}$, and $\hat{\mathcal{P}}_{zk}$.

Modal Identities

Table 9 shows the estimates of the individual terms, $\hat{\mathfrak{M}}^k_{xx}$, and the sum pertaining to the modal identity, $\Sigma_{k=1}^{n} \mathfrak{M}^k_{xx} \leq m$. The comparison between the estimated and calculated values of $\mathfrak{M}^k_{xx}$ is excellent for all the modes except for mode 6 which is a weak mode (i.e., a mode with low response amplitude). The sums also compare very well. In a test situation, the mass of the structure can be assumed to be available in advance. Thus, if a main mode (or modes) was missed in a test, it would be detected by comparing the estimation of $\Sigma_{k=1}^{n} \mathfrak{M}^k_{xx}$ to m. It is observed that the modes 1, 2, and 3 account for over 99.6% of the sum. In other words, modes 1, 2, and 3 account for the bulk of the modal linear momentum in the Ox direction.

Table 10 lists the individual terms, $\mathfrak{M}^k_{yy}$, and the sum. It is observed that modes 1, 2, and 3 account for over 99.6% of the modal linear momentum in the the Oy direction. Table 11 lists the individual terms, $\mathfrak{M}^k_{zz}$, and the sum. It is observed that modes 4, 7, and 8 account for over 99.3% of the modal linear momentum in the Oz direction.

Although the $\mathfrak{M}^k$ are positive if damping is zero, some of them turn out to be negative with nonzero damping (Tables 9–11). This occurs when the angle of the vector representing the complex quantity $\lambda_k Q_k \mathcal{P}_k^2$ is between 90 and 270 deg [Eq. (28)]. This angle arises through the summation of $\angle \lambda_k$, $\angle R_k^d$, and twice $\angle \mathcal{P}_k$. Except in cases of unusually high damping, $\angle \lambda_k$ is close to 90 deg and $\angle Q_k$ is close to -90 deg; thus, the angle of $\lambda_k Q_k \mathcal{P}_k^2$ is very likely to be approximately equal to twice the angle of $\mathcal{P}_k$. So, a negative $\mathfrak{M}^k$ can be expected to occur when $\angle \mathcal{P}_k$ is between approximately 45 and 135 deg. Now, since this angle results from subtracting $\angle R_k^d$ from $\angle B_k^d$ [Eqs. (18), (24), and (26)], a negative $\mathfrak{M}^k$ is likely to occur when $\angle B_k^d$ is lower than ap-

Table 7 Estimates $\hat{\mathcal{P}}_{xk}$ as deduced from driven-base tests (Ox direction) and modal survey tests—comparison of $\mathcal{P}_{xk}$ as calculated by the finite-element model

	Amplitude			Phase, deg		
Mode	$\lvert\mathcal{P}_{xk}\rvert$	$\lvert\hat{\mathcal{P}}_{xk}\rvert$	Error, %	$\angle \mathcal{P}_{xk}$	$\angle \hat{\mathcal{P}}_{xk}$	Diff.
1	3.123	3.123	0.0	179.91	179.91	0.00
2	3.233	3.233	0.0	5.07	5.10	0.03
3	0.2968	0.2968	0.0	4.36	4.35	−0.01
4	0.1167	0.1166	−0.1	181.15	181.17	0.02
5	0.03874	0.03879	0.1	83.35	83.37	0.02
6	0.01175	0.01174	−0.1	39.68	39.76	0.08
7	0.03960	0.03959	0.0	−0.94	−1.03	−0.09
8	0.0008197	0.0008219	0.3	99.22	99.18	−0.04
9	0.001632	0.001634	0.1	96.32	96.26	−0.06

Table 8 Estimates $\hat{\mathcal{P}}_{xk}$, $\hat{\mathcal{P}}_{yk}$, and $\hat{\mathcal{P}}_{zk}$

	X direction		Y direction		Z direction	
Mode	$\lvert\hat{\mathcal{P}}_{xk}\rvert$	$\angle \hat{\mathcal{P}}_{xk}$	$\lvert\hat{\mathcal{P}}_{yk}\rvert$	$\angle \hat{\mathcal{P}}_{yk}$	$\lvert\hat{\mathcal{P}}_{xk}\rvert$	$\angle \hat{\mathcal{P}}_{zk}$
1	3.123	179.91	5.169	−178.83	0.02891	5.62
2	3.233	5.10	2.102	−175.74	0.1645	5.21
3	0.2968	4.35	0.3123	−4.47	0.002496	124.05
4	0.1166	181.17	0.06582	−0.74	2.006	0.00
5	0.03879	83.37	0.005592	168.05	0.08494	−176.60
6	0.01174	39.76	0.01018	−80.50	0.02186	−9.91
7	0.03959	−1.03	0.02136	2.64	0.3121	−0.63
8	0.0008219	99.18	0.02377	171.37	0.09709	0.69
9	0.001634	96.26	0.004166	62.45	0.008622	−178.20

Table 9 Estimates $\hat{\mathfrak{M}}^k_{xx}$ and comparison with theoretical results

Mode	$\mathfrak{M}^k_{xx}$	$\hat{\mathfrak{M}}^k_{xx}$	Error, %	$\mathfrak{M}^k_{xx}/m$	$\hat{\mathfrak{M}}^k_{xx}/m$
1	0.5418	0.5417	0.0	0.2258	0.2257
2	1.671	1.670	−0.1	0.6962	0.6958
3	0.1777	0.1777	0.0	0.07404	0.07404
4	0.006767	0.006760	−0.1	0.002820	0.002817
5	−0.001495	−0.001497	−0.1	−0.0006229	−0.0006238
6	0.00002135	0.00001987	−6.9	0.000008896	0.000008279
7	0.004725	0.004726	0.0	0.001969	0.001969
8	−0.000005821	−0.000005845	−0.4	−0.000002425	−0.000002435
9	−0.000004338	−0.000004351	−0.3	−0.000001808	−0.000001813
Σ	2.400	2.399	0.1	1.000	0.9997

Table 10 Estimates $\hat{\mathfrak{M}}^k_{yy}$ and comparison with theoretical results

Mode	$\mathfrak{M}^k_{yy}$	$\hat{\mathfrak{M}}^k_{yy}$	Error, %	$\mathfrak{M}^k_{yy}/m$	$\hat{\mathfrak{M}}^k_{yy}/m$
1	1.482	1.482	0.0	0.6175	0.6175
2	0.7075	0.7073	0.0	0.2948	0.2947
3	0.2025	0.2024	0.0	0.08437	0.08433
4	0.002157	0.002157	0.0	0.0008988	0.0008988
5	0.00002864	0.00002855	−0.3	0.00001193	0.00001190
6	−0.0004440	−0.0004435	0.1	−0.0001850	−0.0001848
7	0.001359	0.001360	0.1	0.0005662	0.0005667
8	0.005281	0.005271	−0.2	0.002200	0.002196
9	−0.00001738	−0.00001741	−0.2	−0.000007242	−0.000007254
Σ	2.400	2.400	0.0	1.000	1.000

Table 11 Estimates $\hat{\mathfrak{M}}^k_{zz}$ and comparison with theoretical results

Mode	$\mathfrak{M}^k_{zz}$	$\hat{\mathfrak{M}}^k_{zz}$	Error, %	$\mathfrak{M}^k_{zz}/m$	$\hat{\mathfrak{M}}^k_{zz}/m$
1	0.00004534	0.00004535	0.1	0.00001889	0.00001890
2	0.004323	0.004323	0.0	0.001801	0.001801
3	−0.000003767	−0.000003707	1.6	−0.000001570	−0.000001545
4	2.002	2.006	0.2	0.8342	0.8358
5	0.007605	0.007618	0.2	0.003169	0.003174
6	0.002304	0.002270	−1.5	0.0009600	0.0009458
7	0.2945	0.2935	−0.3	0.1227	0.1223
8	0.08877	0.08887	0.1	0.03699	0.03703
9	0.0001245	0.0001244	−0.1	0.00005187	0.00005183
Σ	2.400	2.403	0.1	1.000	1.001

Table 12 Estimates of cross-axis terms, $\hat{\mathfrak{M}}^k_{xy}$, $\hat{\mathfrak{M}}^k_{xz}$, and $\hat{\mathfrak{M}}^k_{yz}$

Mode	$\hat{\mathfrak{M}}^k_{xy}$	$\hat{\mathfrak{M}}^k_{xz}$	$\hat{\mathfrak{M}}^k_{yz}$
1	0.8960	−0.004981	−0.008221
2	−1.087	0.08500	−0.05531
3	0.1919	−0.001064	−0.0009263
4	−0.003821	−0.1164	0.06575
5	−0.00009617	−0.0005729	0.0004849
6	0.0004906	0.0009704	0.0001565
7	0.002540	0.03724	0.02001
8	0.00002180	−0.0002095	−0.02193
9	−0.00001078	0.000004028	−0.00002458
Σ	0.245 *E*-4	−0.130 *E*-4	−0.105 *E*-4
Σ_{theo}	0.771 *E*-7	−0.450 *E*-8	0.882 *E*-9

proximately 45 deg and greater than approximately −45 deg. Since the angle of B^q_k is fairly close to 90 deg (or −90 deg) for a strong mode and a response location away from a node, then $\mathfrak{M}^k$ will be positive. A negative $\mathfrak{M}^k$ is then likely to appear only for a weak mode containing a low modal linear momentum, and can therefore be expected to have no significant effect on $\Sigma^n_{k=1}\mathfrak{M}^k$. This phenomenon is observed with the present example.

Table 12 lists the cross-axis terms, $\hat{\mathfrak{M}}^k_{xy}$, $\hat{\mathfrak{M}}^k_{xz}$, and $\hat{\mathfrak{M}}^k_{yz}$ and their sums. The data of the table agree with the expectations of the theoretical results, Eq. (27), after allowing for errors in the estimation process.

IV. Driven-Base Tests with Translational and Rotational Excitation

Six-Degree-of-Freedom Excitation

Consider a test where the base is driven by three translational and three rotational periodic motions, with equipment as described in Ref. 1, for example. The measureable input variables are assumed to be the three accelerations of the center of rotation of the base (a_{ox},a_{oy},a_{oz}) and the three angular accelerations $(\alpha_{ox},\alpha_{oy},\alpha_{oz})$ of the base about the axes $(Oxyz)$ that are attached to the block with 0 at the center of rotation. The measureable output variables are assumed to be the accelerations (A_x,A_y,A_z), as before. The modal model for this configuration may be shown to have the following form:

$$\begin{aligned}\bar{A}_x - \bar{a}_{ox}\Sigma + (\bar{\alpha}_{oz}Y - \bar{\alpha}_{oy}Z) &= \sum_{k=1}^{n} \frac{\omega^2\theta_k}{(i\omega-\lambda_k)} Q_k(\mathcal{P}_{xk}\bar{a}_{ox} + \mathcal{P}_{yk}\bar{a}_{oy} + \mathcal{P}_{zk}\bar{a}_{oz} \\ &+ \mathcal{H}_{xk}\bar{\alpha}_{ox} + \mathcal{H}_{yk}\bar{\alpha}_{oy} + \mathcal{H}_{zk}\bar{\alpha}_{oz}) \\ &+ \sum_{k=1}^{n} \frac{\omega^2\theta^*_k}{(i\omega-\lambda^*_k)} Q^*_k(\mathcal{P}^*_{xk}\bar{a}_{ox} + \mathcal{P}^*_{yk}\bar{a}_{oy} + \mathcal{P}^*_{zk}\bar{a}_{oz} \\ &+ \mathcal{H}^*_{xk}\bar{\alpha}_{ox} + \mathcal{H}^*_{yk}\bar{\alpha}_{oy} + \mathcal{H}^*_{zk}\bar{\alpha}_{oz}) \end{aligned} \tag{29}$$

together with two additional equations obtainable by permuting $(A_x\rightarrow A_y\rightarrow A_z)$, $(X\rightarrow Y\rightarrow Z)$, $(\theta_k\rightarrow\phi_k\rightarrow\psi_k)$, etc. The above X, Y, and Z are $N\times 1$ column matrices giving locations of the N mass points relative to $(Oxyz)$, and the $\mathcal{H}$ are modal angular momentum coefficients. $\mathcal{H}_{xk}$ is given by

$$\mathcal{H}_{xk} = Y^T M^N \psi_k - Z^T M^N \phi_k \triangleq \sum_{i=1}^{N} m^i (y^i\psi^i_k - z^i\phi^i_k) \tag{30}$$

and $\mathcal{H}_{yk}$ and $\mathcal{H}_{zk}$ can be obtained from this expression by permitting symbols $x\rightarrow y\rightarrow z$, etc.

Estimation might be possible from this rather complex modal model, but it would require development beyond what has presently been achieved. Of more immediate significance, however, is the appearance of the modal angular momentum coefficients.

Single-Degree-of-Freedom Rotational Excitation

For a driven-base test with single-degree-of-freedom rotational input about the Ox axis, Eq. (29) has $\alpha_{ox}\neq 0$,

$a_{ox}=a_{oy}=a_{oz}=\alpha_{oy}=\alpha_{oz}=0$ and reduces to

$$\begin{bmatrix} \bar{A}_x(\omega)/\bar{\alpha}_{ox}(\omega) \\ \bar{A}_y(\omega)/\bar{\alpha}_{ox}(\omega)+X \\ \bar{A}_z(\omega)/\bar{\alpha}_{ox}(\omega)-Y \end{bmatrix} = \omega^2 \sum_{k=1}^{n} \left\{ \frac{Q_k \mathcal{IC}_{xk} \Phi_k}{i\omega-\lambda_k} + \frac{Q_k \mathcal{IC}^*_{xk} \Phi^*_k}{i\omega-\lambda^*_k} \right\} \tag{31}$$

Equation (31) has a structure similar to Eq. (11). Thus, by analogy with results reported in the previous sections, it may be concluded that a driven-base test with single-degree-of-freedom rotational excitation about Ox offers the opportunity to estimate $(Q_k \mathcal{IC}_{xk})$, as well as λ_k and Φ_k. When combined with a modal survey test that estimates the Q_k, experimental estimates for the $\mathcal{IC}_{xk}$ can be further calculated. The estimates of $\mathcal{IC}_{xk}$ then make possible the use of the modal identities of the form

$$\sum_{k=1}^{n} \{\lambda_k Q_k \mathcal{IC}^2_{xk} + \lambda^*_k Q^*_k \mathcal{IC}^{*2}_{xk}\} \leq I_{xx} \tag{32}$$

[where I_{xx} is the moment of inertia of the flexible structure about Ox (Refs. 6 and 7)] to assess the relative significance and overall completeness of the modes in the manner illustrated in the previous work with the $\mathcal{P}_k$.

V. Uses for Estimated Momentum Coefficients

The potential use of experimentally derived estimates of $\mathcal{P}$ and $\mathcal{IC}$ warrants description.

One application is in combination with the modal identities for assessment of significance and completeness of modes, as is described in the foregoing. This type of calculation is sometimes done for analytically-derived modes, using a version of the identities derived on the basis of undamped modal theory. The application of modal identities is illustrated in a test situation in Ref. 11, wherein the $\mathfrak{M}$ are calculated using measured mode shapes and an analytical mass matrix.

Being experimentally derivable parameters, the estimates of $\hat{\mathcal{P}}_k$ or $\widehat{(Q_k \mathcal{P}_k)}$ can be used to validate an analytical model of a structure by comparison to corresponding analytically calculated quantities. As the $\hat{\mathcal{P}}_k$ are closely related to reaction forces at mounting points of the structure, they may validate load and stress aspects of an analytical model better than is achievable through comparison of modal frequencies and shapes.

In the differential equations that describe dynamics and control of flexible satellites in orbit, $\mathcal{P}$ and $\mathcal{IC}$ corresponding to flexible substructures around attachment points appear as parameters (for example, in Ref. 12). For this reason, these quantities are often used to specify flexible properties of substructures by contracting organizations instead of or in addition to mode shapes and mass distribution. Whereas these particular parameters are usually calculated with an analytical model, the driven-base test offers the opportunity to measure them directly.

VI. Conclusions

The work demonstrates that the driven-base test offers the potential to estimate the product (momentum coefficient $\times$ scale factor), in addition to natural frequency, damping factor, and shape for each mode. Tests with translational driven-base input lead to estimation of linear momentum coefficients. Tests with rotational driven-base input lead to estimation of angular momentum coefficients.

If, in addition, estimates of modal scale factors are obtained from an independent modal test or from an analytical model, then estimates of momentum coefficients can be constructed. In principle, for each mode, output measurements from a single well chosen point (i.e., one response function) on the structure suffice to enable estimates of the modal momentum coefficients. The modal momentum coefficients can be used, in conjunction with modal identities, to assess the relative significance and overall completeness of experimentally-determined modes.

The concepts in this paper are demonstrated using a computer-simulated structure. Previous work[2,3] has demonstrated estimation of modal frequencies, damping factors, and mode shapes with real structures. The demonstration with real structures, of estimation of modal momentum coefficients, of rotational base excitation, and of other concepts in this paper seems straightforward and will be reported in future publications.

References

[1] *Spacecraft Vibration Testing Using Multiaxis Hydraulic Vibration Systems*, edited by W. R. Burke, ESA SP-197, Proceedings of a ESTEC Workshop, Noordwijk, the Netherlands, May, 1983.

[2] Béliveau, J.-G., Vigneron, F. R., Soucy, Y., and Draisey, S., "Modal Parameter Estimation from Base Excitation," *Journal of Sound and Vibration*, Vol. 107, No. 3, June 1986, pp. 435-449.

[3] Draisey, S., Vigneron, F. R., Soucy, Y., and Béliveau, J.-G., "Modal Parameter Estimation From Driven-Base Tests," *Second International Symposium on Aeroelasticity and Structural Dynamics*, Paper 85-39, Aachen, West Germany, April 1985.

[4] Ewins, D. J., *Modal Testing: Theory and Practice*, John Wiley and Sons, 1984.

[5] Brown, D. L., "Modal Analysis Short Course Notes," Section 13, Analytical and Experimental Analysis, Structural Dynamics Research Laboratory, University of Cincinnati, Cincinnati, OH, 1984.

[6] Vigneron, F. R., "A Natural Modes Formulation and Modal Identities for Structures with Linear Viscous Damping," CRC Rept. 1382, Department of Communications, Ottawa, Canada, Jan. 1985.

[7] Vigneron, F. R., "A Natural Modes Model and Modal Identities for Damped Linear Structures," *ASME Journal of Applied Mechanics*, Vol. 53, No. 1, March 1986, pp. 33-38.

[8] Vold, H., Kundrat, J., Rocklin, G. T., and Russell, R., "A Multi-Input Modal Estimation Algorithm for Minicomputers," SAE Technical Paper Series (820194), 1982.

[9] Leuridan, J. and Vold, H., "A Time-Domain Linear Modal Estimation Technique For Multiple Input Modal Analysis," *Modal Testing and Modal Refinement*, ASME, AMD-Vol. 59, 1983, pp. 51-62.

[10] Allemang, R. J. and Brown, D. L., "A Correlation Coefficient for Modal Vector Analysis," *Proceedings of the Ist International Modal Analysis Conference*, Orlando, FL, Nov. 1982, pp. 110-116.

[11] Wada, B. K., Garba, J. A., and Chen, J. C., "Development and Correlation: Viking Orbiter Analytical Dynamic Model With Modal Test," *The Shock and Vibration Bulletin*, No. 44, Aug. 1974, pp. 125-164.

[12] Hughes, P. C., "Modal Identities for Elastic Bodies, With Application to Vehicle Dynamics and Control," *Journal of Applied Mechanics*, Vol. 47, March 1980, pp. 177-184.